Journal of Energetic Materials
Publication details, including instructions for authors and subscription information:
http://www.informaworld.com/smpp/title~content=t713770432

Synthesis and Characterization of Furazan Energetics ADAAF and DOATF

Jacqueline M. Veauthier[a]; David E. Chavez[a]; Bryce C. Tappan[a]; Damon A. Parrish[b]
[a] Chemistry and Weapon Experiments Materials Divisions, Los Alamos National Laboratory, Los Alamos, New Mexico, USA [b] Naval Research Laboratory, Laboratory for the Structure of Matter, Washington, DC, USA

Online publication date: 08 June 2010

To cite this Article Veauthier, Jacqueline M. , Chavez, David E. , Tappan, Bryce C. and Parrish, Damon A.(2010) 'Synthesis and Characterization of Furazan Energetics ADAAF and DOATF', Journal of Energetic Materials, 28: 3, 229 — 249
To link to this Article: DOI: 10.1080/07370651003601769
URL: http://dx.doi.org/10.1080/07370651003601769

Journal of Energetic Materials, 28: 229–249, 2010
ISSN: 0737-0652 print/1545-8822 online
DOI: 10.1080/07370651003601769

Taylor & Francis
Taylor & Francis Group

Synthesis and Characterization of Furazan Energetics ADAAF and DOATF

JACQUELINE M. VEAUTHIER,[1]
DAVID E. CHAVEZ,[1] BRYCE C. TAPPAN,[1]
and DAMON A. PARRISH[2]

[1]Chemistry and Weapon Experiments Materials Divisions, Los Alamos National Laboratory, Los Alamos, New Mexico, USA
[2]Naval Research Laboratory, Laboratory for the Structure of Matter, Washington, DC, USA

The synthesis and structural characterization of bis[4-aminofurazanyl-3-azoxy]azofurazan (ADAAF) and 3,4:7,8:11,12:15,16-tetrafurazano-1,2,5,6,9,10,13,14-octaazacyclohexadeca-1,3,5,7,9,11,13,15-octaene-1,10-dioxide (DOATF) are described. Explosive sensitivity properties of both materials were determined. The heat of formation of ADAAF was measured to be 300 kcal/mol and the detonation velocity and pressure of ADAAF were measured to be 7.88 km/s and 299 kbar, respectively, at 94% theoretical maximum density. We also investigated the burning rate characteristics of ADAAF.

Keywords: burning rate, furazan, heat of formation, performance, sensitivity

Address correspondence to Jacqueline M. Veauthier, Chemistry and Weapon Experiments Materials Divisions, Los Alamos National Laboratory, MS J582, Los Alamos, NM 87545. E-mail: veauthier@lanl.gov

Introduction

In 1968, M. D. Coburn reported the first synthesis of 3,4-diamino furazan, **1** [1]. Since then, several new energetic molecules derived from the oxidation of **1** have appeared in the literature [2–13]. A few examples of these compounds are shown in Fig. 1 (**2**–**5**). We became interested in these materials because of their predicted and measured high heats of formation in addition to the appealing sensitivity properties that have been reported for **2** and **3**. The synthesis of 3,3′-diamino-4,4′-azoxyfurazan (DAAF, **3**) was first reported by Russian scientists in 1981 [2] and later improved by members of our laboratory [10]. This improved synthetic procedure has facilitated efforts by our team to prepare and characterize new derivatives of DAAF. Although there are literature reports by Russian and Chinese scientists on the synthesis of the dioxoazotetrafurazan (DOATF, **5**), measured sensitivity and performance data are not available on this material [9,13]. Russian scientists also report azodiaminoazoxyfurazan (ADAAF, **4**) as a precursor to **5** but do not provide details on the sensitivity properties of **4** [9,11]. We now describe the synthesis, structural properties, and sensitivity data for compounds **4** and **5**. Additionally, we executed small-scale performance tests and now report the detonation velocity, detonation pressure, and burning rate properties of **4**.

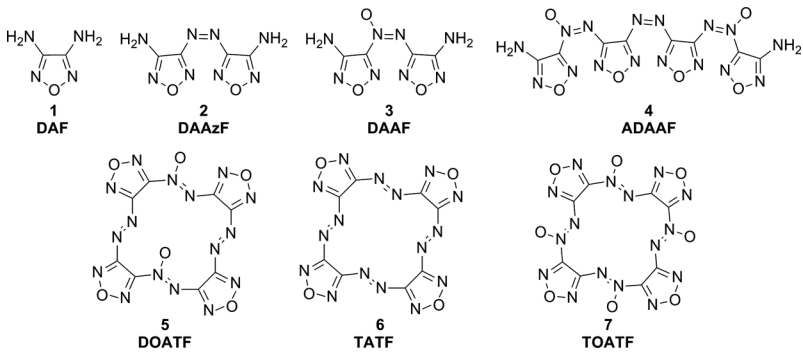

Figure 1. 3,4-Diaminofurazan (DAF, **1**) and examples of its oxidation products (**2**–**5**).

Results and Discussion

Synthesis

There are reports by Russian and Chinese scientists that describe the synthesis of the diazene oxide macrocycle **5** [9]. These methods utilize either **3** or **4** as the starting material and either lead (IV) acetate [$Pb(OAc)_4$] or dibromoisocyanuric acid (DBI) as the oxidant. If **4** is the starting material, the primary product is **5**, whereas with **3**, both the 1,10-dioxide (**5**) and the 1,9-dioxide macrocycles form. Because it proved difficult to separate the two dioxide macrocyclic products, we focused our efforts on the synthesis of **5** from **4**. First, it was necessary to find a synthetic route to **4**. We found that treatment of two equivalents of **3** with two equivalents of $KBrO_3$ in glacial acetic acid at 50°C for 16 h gave ADAAF (**4**) as an analytically pure yellow precipitate in 60% yield (Scheme 1). Sheremetev et al. have reported a similar synthesis of **4** with hydrochloric acid in a recent patent application [11].

For the synthesis of **5**, we found that treatment of **4** with DBI in acetonitrile at ambient temperatures did result in formation of **5** as reported by Eman et al. [9]. However, DBI is not commercially available, its synthesis requires the use of significant amounts of highly toxic bromine, and it decomposes when exposed to light and moisture; therefore, we investigated the use of alternative oxidants for the preparation of **5**. Trichloroisocyanuric acid (TCI) is commercially available and has been used for the oxidation of primary amines [10,14]. Indeed, we now report that one equivalent of **4** in dilute CH_3CN reacts with 1.9 equivalents of TCI at ambient temperatures to yield DOATF (**5**) in 26% isolated yield (Scheme 1).

X-Ray Crystallography

To date, there are no published reports on the X-ray crystal structures of **4** or **5**. However, solvent-free X-ray quality crystals of compound **4** can be grown from hot acetonitrile and solvent-free X-ray quality crystals of **5** can be grown from warm toluene. Crystal data and structure refinement parameters for **4**

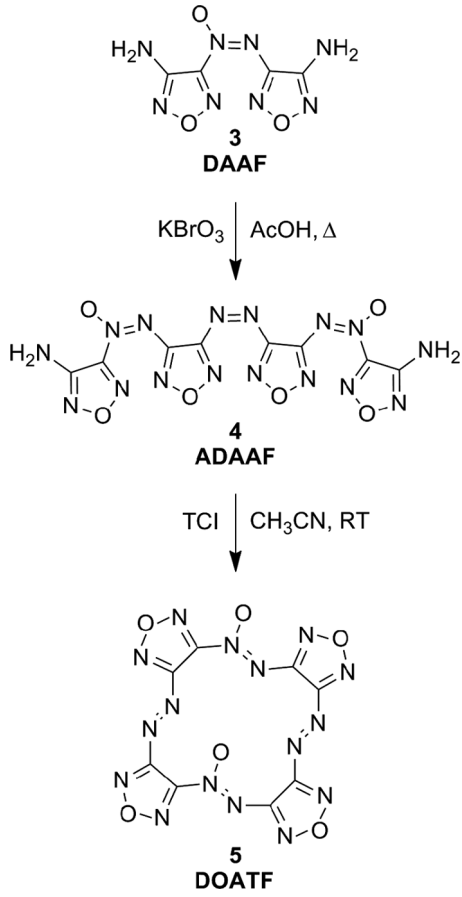

Scheme 1. Synthesis of ADAAF, **2**, and DOATF, **3**.

and **5** are listed in Table 1, selected bond lengths and torsion angles are listed in Table 2, and ORTEP structures are shown in Figs. 2 and 3. The X-ray structure of **4** confirms it to be an azo-bridged diamino azoxyfurazan that is similar to the X-ray structure of DAAF (**3**, [15]); however, in **3** the amino group is oriented on the same side as and hydrogen bonds to the azoxy oxygen, whereas in **4**, the amino group is oriented away from the azoxy oxygen. Both **3** and **4** are relatively planar. For example, in **4** the dihedral angles between the planes defined

Table 1

Crystal data and structure refinement parameters for ADAAF (**4**) and DOATF (**5**)

	4 (ADAAF)	**5** (DOATF)
Empirical formula	$C_8H_4N_{16}O_6$	$C_8N_{16}O_6$
Formula weight	420.27	416.24
Crystal system	Monoclinic	Triclinic
Space group	$P2_1/n$	$P\overline{1}$
a (Å)	11.309(14)	5.7364(2)
b (Å)	11.3388(5)	11.5088(5)
c (Å)	12.7226(5)	12.0378(5)
α (°)	90	96.1030(10)
β (°)	104.11(6)	98.3090(10)
γ (°)	90	101.1660(10)
Volume (Å^3)	1577.60(11)	764.08(5)
Z	4	2
Temperature (K)	113	113
Density (Calcd) (mg/m^3) at 113 K	1.769	1.809
Density (Calcd), (mg/m^3) at 293 K	1.728	1.761
Abs. coeff. (mm^{-1})	0.153	0.157
$F(000)$	848	416

(*Continued*)

Table 1
Continued

	4 (ADAAF)	**5** (DOATF)
θ for data collection	2.15 to 26.42	1.73 to 29.24
Limiting indices	$-14 \leq h \leq 14$	$-7 \leq h \leq 7$
	$-14 \leq k \leq 14$	$-15 \leq k \leq 15$
	$-15 \leq l \leq 15$	$-16 \leq l \leq 16$
Reflections collected	14160	8890
Independent reflections	3234 [R(int) = 0.0235]	4049 [R(int) = 0.0130]
Completeness to $2\theta = 50.00°$	99.8%	97.7%
Refinement method	Full-matrix least-squares on F^2	Full-matrix least-squares on F^2
Data/restraints/parameters	3234/0/271	4049/0/271
Goodness-of-fit on F^2	1.023	1.028
Final R indices ($I > 2\sigma I$)	R1 = 0.0329, wR2 = 0.0861	R1 = 0.0344, wR2 = 0.0960
R indices (all data)	R1 = 0.0380, wR2 = 0.0897	R1 = 0.0380, wR2 = 0.0991
Largest diff. peak and hole	0.322 and −0.331 e. $Å^{-3}$	0.376 and −0.194 e. $Å^{-3}$

Table 2
Selected bond lengths (Å) and torsion angles (°) for ADAAF (**4**) and DOATF (**5**)

	4		**5**
N21–N20	1.288(2)	N13–N14	1.256(2)
N13–N14	1.260(2)	N9–N10	1.272(1)
N6–N7	1.287(2)	N5–N6	1.258(1)
		N1–N2	1.276(1)
N21–O21	1.241(2)	N1–O1	1.242(1)
N6–O6	1.243(2)	N10–O10	1.247(1)
N23-C22-N21-N20	178.42	N12-C12-N13-N14	162.91
N18-C19-N20-N21	1.93	N11-C11-N10-N9	−112.84
N16-C15-N13-N14	−175.64	N15-C15-N14-N13	17.28
N11-C12-N13-N14	176.57	N16-C16-N1-N2	−129.74
N9-C8-N7-N6	7.11	N3-C3-N2-N1	−120.33
N4-C5-N6-N7	175.75	N4-C4-N5-N6	−169.28
		N7-C7-N6-N5	38.16
		N8-C8-N9-N10	−136.46

by furazan rings D and C and furazan rings D and A are 4.3 and 5.1°, respectively, and the dihedral angle between D and the plane defined by C5-N6-N7 is 4.3° (cf. for **3**, the dihedral angle between the furazan rings is 0.0°, whereas the dihedral angle

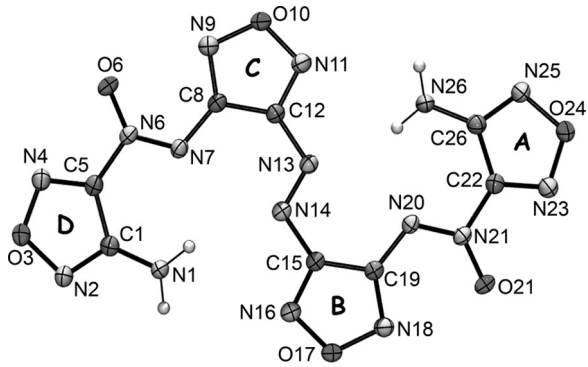

Figure 2. Thermal ellipsoid representation of ADAAF, **4** (50% probability ellipsoids).

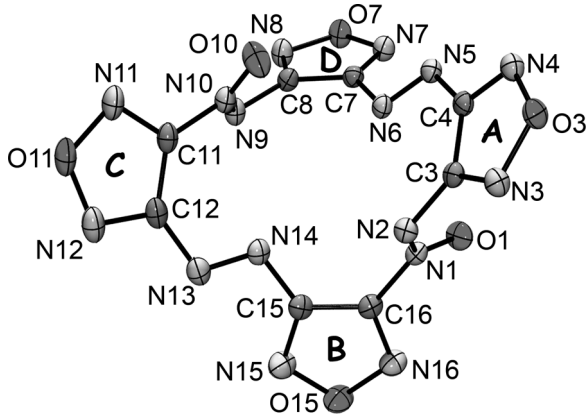

Figure 3. Thermal ellipsoid representation of DOATF, **5** (50% probability ellipsoids).

between the furazan ring and the azoxy group is 6.7°). This is further evidenced by the torsion angles for **4** that are listed in Table 2 that are either less than 10° or greater than 170°. The X-ray crystal density for **4** at ambient temperatures is 1.728 g/cm^3 compared to 1.745 g/cm^3 for **3** [15]. At 113 K, the density of **4** is 1.769 g/cm^3 and is comparable to the calculated value of 1.76 g/cm^3 reported in the Russian patent [11]. The azoxy N−N bond lengths in **4** are 1.288(2) Å and 1.287(2) Å compared to 1.280 Å for **3**. The azo N−N bond length for **4** is slightly shorter at 1.260(2) Å. The X-ray structure of **5** confirms this molecule to be an azo- and azoxy-bridged tetrafurazan macrocycle that is nonplanar. More specifically, the torsion angles between the azo and azoxy groups and their neighboring C–N furazan bonds are between 17.3 and 169.3° (Table 2) and the dihedral angles between the planes defined by furazan rings are 67.3, 32.2, 67.8, 45.6, 82.9, and 77.9° (A-B, B-C, C-D, D-A, D-B, and A-C, respectively). This type of distortion has also been reported for the X-ray structures of the all azo derivative of **5**, TATF, and the all azoxy derivative of **5**, TOATF, shown in Fig. 1 [8,9]. The X-ray crystal density for **5** at 113 K is 1.809 g/cm^3 compared to 1.791 g/cm^3 at 153 K for TATF [8] and 1.935 g/cm^3 at 183 K for TOATF [9]. The azoxy N−N bond

lengths for **5** are 1.276(1) Å and 1.272(1) Å, and the azo N−N bond lengths are slightly shorter at 1.258(1) Å and 1.256(2) Å (cf. azo N−N, 1.253 for TATF [8]).

Explosive Properties

We have tested ADAAF (**4**) and DOATF (**5**) for thermal, impact, friction, and spark sensitivities (see Table 3). Differential scanning calorimetry (DSC) confirms that **4** begins to decompose near 227°C with a peak exotherm at 266°C and an energy release of 3022 J/g, whereas the patent application by Sheremetev et al. reported a decomposition temperature of 267°C for **4** [11]. The DSC trace for **5** reveals a melt at 127°C and **5** appears to be stable in the melt and only begins to decompose at 212°C, with a peak exotherm that occurs at 289°C with an energy release of 3089 J/g. It is interesting to note that in the Chinese literature [13] the melting point of DOATF is reported to be 93°C and in other Russian literature [9] the corresponding melting point is reported to be 144°C. For comparison, the published DSC onset for pure DAAF (**3**) is 248°C [10]. We used

Table 3
Small-scale sensitivity data for ADAAF (**4**) and DOATF (**5**)

	Impact (cm)	Friction (kg)	Spark (J)	DSC (°C)
4	36.2	26	0.0625	227 (onset) 266 (exo)
5	11.2	4.7	0.125	127 (endo, mp) 212 (onset) 289 (exo)
PETN[a]	15.1	7.0	0.0625	140 (endo, mp) 159 (onset) 205 (exo)

[a]PETN type RPS 3518 was the standard for impact, spark, and friction tests, and PETN type 94-01B was the standard for DSC thermal analysis.

combustion calorimetry to determine the heat of formation (ΔH_f) of **4**. We found $\Delta H_f = 300$ kcal/mol for **4**, which is extremely large when compared to DAAF (i.e., $\Delta H_f = 106$ kcal/mol for **3** [10]) and could be attributed, in part, to the presence of two additional N=N bonds in **4**. This high ΔH_f value is much higher than that reported in the patent by Sheremetev et al. for **4** ($\Delta H_f = 237$ kcal/mol, calculated [11]). To date, we have not measured ΔH_f for **5** because of its high sensitivity to friction (see Table 3) and the associated safety hazard of pressing this material into pellets for combustion studies.

We found that oxidation of compound **3** to **4** and then **4** to **5** result in significantly increased sensitivities to mechanical stimuli (Table 3). For example, compound **3** is insensitive to both impact and friction [10], whereas **4** and **5** have impact sensitivities of 36.2 and 11.2 cm, respectively, and friction sensitivities of 26 and 4.7 kg, respectively. However, **3**–**5** are all only slightly sensitive to spark. Although more detailed experiments are necessary to understand why there are dramatic differences in mechanical sensitivities between **3**–**5**, a crude examination of the crystal packing for **4** and **5** compared to that of **3** and the related material DAAzF (**2**) [16] does reveal noteworthy differences (see Fig. 4). For example, the relatively insensitive molecules DAAzF (**2**) and DAAF (**3**) pack into layered structures, which is similar to that of the well-known insensitive high-explosive TATB (1,3,5-triamino-2,4,6-trinitrobenzene) [17]. In this type of packing structure, the layers can easily slip or slide, which may make it difficult to form hot spots in these materials. In contrast, the packing diagrams for ADAAF (**4**) and DOATF (**5**) do not reveal any type of layering that would permit significant sliding between molecular layers. Additionally, it is interesting to note that **2** and **3** each have a more negative oxygen balance than either **4** or **5** and **4** is less balanced than **5**. Work is ongoing to help us gain a better understanding of these differences.

Next, we measured the detonation velocity and detonation pressure of neat ADAAF (**4**). For comparison, neat DAAF has been reported to have a detonation velocity (D_v) of 7.89 km/s and detonation pressure (P_{CJ}) of 291 kbar (0.5-in.

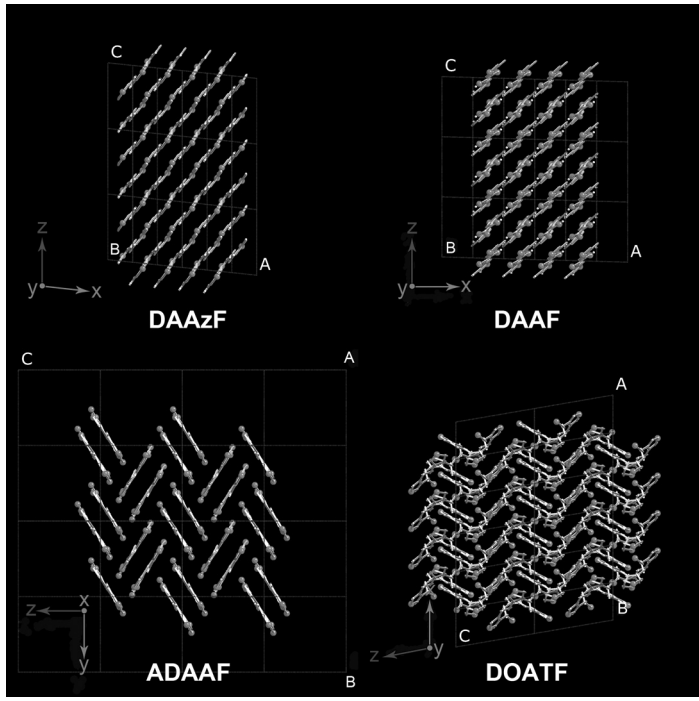

Figure 4. Molecular packing diagrams for DAAzF, **2** (top left) [16]; DAAF, **3** (top right) [17]; ADAAF, **4** (bottom left); and DOATF, **5** (bottom right).

rate stick of pellets at 95% TMD) [10c]. We prepared an unconfined rate stick of pellets of ADAAF at a density of 1.63 g/cm^3 (94% TMD) and 0.5-in. diameter. A complete detonation was confirmed by the witness plate and the detonation pressure (P_{CJ}) was estimated to be 299 kbar from a 0.092-in.-diameter plate dent depth. The detonation velocity was determined from the slope of a plot of detonation front distance vs. time and was found to be 7.88 km/s (Fig. 5). In addition, CHEETAH 4.0 [18] was used to predict the explosive performance of **4**. Using the experimentally determined values for theoretical maximum density (1.73 g/cm^3) and ΔH_f, a detonation velocity of 8.28 km/s and a detonation pressure of 279 kbar are predicted. If the density is lowered to 94% TMD

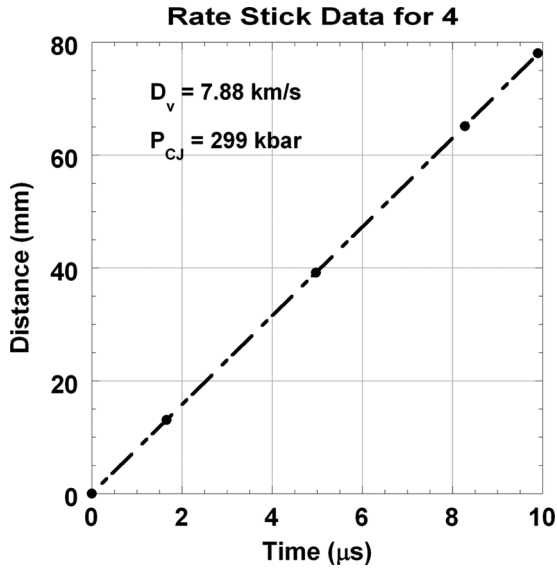

Figure 5. Rate stick of ADAAF, **4**, at a pellet density of 1.63 g/cm^3 (94% TMD).

(1.63 g/cm^3), a detonation velocity of 7.89 km/s and detonation pressure of 244 kbar are predicted by CHEETAH 4.0. Sheremetev et al. reported calculated values for detonation velocity and pressure or 8.09 km/s and 298 kbar, respectively (although it seems that these values were calculated at a theoretical density of 1.76 g/cm^3) [11]. We have not measured the explosive performance of DOATF (**5**); however, Chinese scientists have reported a calculated detonation velocity of 8.2 km/s and a calculated detonation pressure of 292 kbar for **5** [13].

Burning Rate Measurements

The burning rates of 0.25-in. × 0.25-in. cylindrical pellets of ADAAF (**4**, 93–94% TMD) were measured in a pressurized combustion chamber filled with nitrogen between 0.3 and 7 MPa and the results are listed in Table 4. The burning rate is determined by measuring the distance of the flame front over time. Typical images used to track the flame front are shown in

Table 4
Burning rate data for ADAAF, **4**

Pellet density (g/cm^3)	Pressure (MPa)	Burning rate (cm/s)
1.644	6.87	1.85
1.651	5.56	1.53
1.658	4.16	1.29
1.649	2.81	1.08
1.661	1.37	0.50
1.642	0.35	0.15

Fig. 6. The pressure-dependent burning rates of **4** are plotted in Fig. 7 with those of HMX (93% TMD [19]) and DAAF (97% TMD [19]) for comparison. The data suggest that under the experimental conditions investigated, ADAAF (**4**) burning is similar to the conventional explosive, HMX, given that the burning rate equations of **4** and HMX are well matched [19]. When compared to its high-nitrogen precursor, DAAF, ADAAF burns at a faster rate than DAAF and with slightly

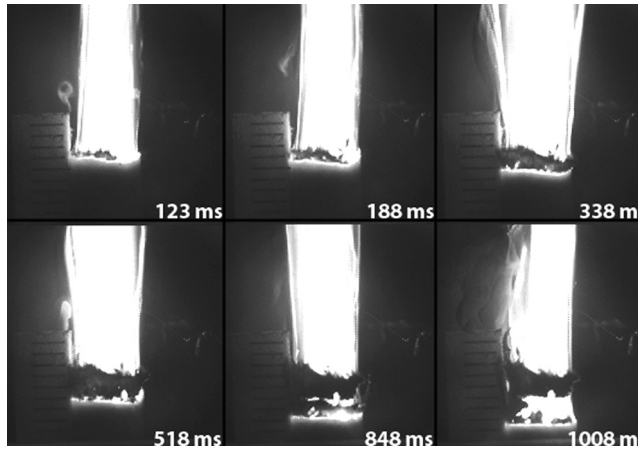

Figure 6. Frame sequence of burning ADAAF, **4**, at 1.37 MPa, filmed at 200 f/s. The flame front is moving from top to bottom.

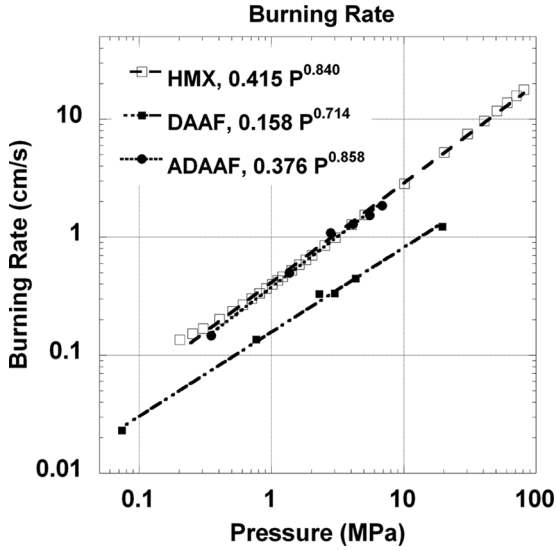

Figure 7. Burning rate characteristics of neat ADAAF (**4**) at 93–94% TMD. For comparison, burning rate data for neat DAAF (**3**, 97% TMD) and neat HMX (93% TMD) are plotted [19].

increased pressure dependence (i.e., the pressure exponents of ADAAF and DAAF are 0.858 and 0.714, respectively). This pressure exponent value is considered high and suggests that the burning rate of ADAAF, like HMX and to a smaller extent DAAF, is pressure dependent and that a significant amount of decomposition of **4** occurs in the gas phase through secondary reactions.

Conclusions

We have reported two new synthetic procedures and the first X-ray crystal structures for the azoxyfurazan compounds ADAAF (**4**) and DOATF (**5**). These new energetic materials were found to be significantly more sensitive to mechanical initiation than DAAF (**3**) and the heat of formation of **4** ($\Delta H_f = 300$ kcal/mol) was found to be nearly three times that of **3** ($\Delta H_f = 106$ kcal/mol). The detonation velocity and pressure for **4** ($D_v = 7.88$ km/

s and $P_{CJ} = 299$ kbar at 94% TMD) are comparable to **3** ($D_v =$ 7.89 km/s and $P_{CJ} = 291$ kbar at 95% TMD), whereas the burning rate characteristics of **4** are similar to HMX. Further studies to elucidate sensitivity behavior are ongoing.

Experimental

> **Caution:** Although we have not experienced any problems in handling the materials described in this article, some of the described compounds are highly sensitive to impact and friction. Therefore, they should be handled with extreme care, implementing standard safety procedures for handling energetic materials.

General

Unless otherwise noted, all starting materials were obtained from commercial sources. DAAF (**3**) can be prepared according to published literature procedures [2,10]. All nuclear magnetic resonance (NMR) spectra were obtained on a JEOL Eclipse+ Delta 300 MHz NMR spectrometer. Elemental analyses were performed at Los Alamos National Laboratory on a Leco CHN 900 Elemental Analyzer. Melting points were determined by DSC on a TA Instruments Q2000 DSC.

X-ray crystal data were collected at the Naval Research Laboratory (Washington, D.C.). Crystal data and structure refinement parameters for **4** and **5** are listed in Table 1. Crystals of **4** ($0.184 \times 0.156 \times 0.126\,mm^3$) and **5** ($0.911 \times 0.566 \times 0.384$ mm^3) were mounted on glass fibers using a small amount of epoxy. Data were collected on a Bruker three-circle platform diffractometer equipped with a SMART 1000 CCD detector. The crystals were irradiated using graphite monochromated MoK_α radiation ($\lambda = 0.71073$). The crystals were collected at 113 K. Data collection was performed and the unit cell of each crystal was initially refined using *SMART* [v5.625] [20]. Data reduction was performed using *SAINT* [v6.45A] [21] and *XPREP* [v6.14] [22]. Corrections were applied for Lorentz, polarization, and absorption effects using *SADABS* [v2.10]

[23]. The structure was solved and refined with the aid of the programs in the *SHELXTL-plus* [v6.12] system of programs [24]. The full-matrix least-squares refinement on F^2 included atomic coordinates and anisotropic thermal parameters for all non-H atoms. The H atoms were included using a riding model.

The Cambridge Crystallographic Data Centre (CCDC) contains the supplementary crystallographic data for this article. These data can be obtained free of charge from CCDC via http://www.ccdc.cam.ac.uk/datarequest/cif.

Small-scale explosive sensitivity safety tests for **4** and **5** were performed using standard procedures. Impact sensitivity was measured by using a drop hammer LANL type 12 test using a 2.5 kg weight and the Bruceton up/down method to determine the 50% drop height. Friction sensitivity was measured by a mini BAM machine (Reichel & Partner, Rhenzabern, Germany) using the Bruceton up/down method to determine the 50% load. Spark sensitivity from 0 to 6 J was measured by an ABL electrostatic discharge apparatus (Safety Management Services, West Jordan, UT) connected to a diagnostic analyzer to detect NOX, CO (0–5,000 ppm), and CO_2 (0–1000 ppm) released from the sample. Thermal decomposition temperatures were measured by DSC (TA Instruments Q2000 DSC) in hermetically sealed aluminum pans that contain a pinhole lid. A typical analysis utilizes approximately 1 mg of sample with 50 mL/min ultra-high-purity nitrogen purge gas at a thermal ramp rate of 10°C/min. All sensitivity data are referenced to a PETN standard. A Parr 6300 Calorimeter was used to determine the heat of formation of **4** from the combustion of 0.25-in. × 0.25-in. cylindrical pellets of **4**.

The detonation velocity of **4** was determined with a 78-cm-length rate stick prepared from 0.5-in. × 0.5-in. cylindrical pellets pressed to a density of ∼1.63 g/cm^3 (94% TMD).

For burning rate measurements, cylindrical pellets 0.25 in. diameter and 0.25 in. long of **4** (93–94% TMD) were burned in a 2-L stainless steel vessel under pressurized nitrogen between 0.3 and 7 MPa. The volume is sufficiently large that the decomposition gases have little effect on the pressure. To prevent the flame front from spreading down the pellet sides,

burning of the pellet sides was inhibited with a thin film of silicon grease. The pellets were ignited by means of a resistively heated nickel chromium wire. The combustion event was filmed between 200 and 400 fps using a Phantom MIRO3 high-speed-video system from Vision Research (Wayne, New Jersey, USA). The pressure was monitored with an Omega Model PX605-10KGI static pressure transducer. Optical records were analyzed using commercially available computer graphics software to obtain the burning rate data.

Bis[4-Aminofurazanyl-3-Azoxy]Azofurazan (ADAAF, 4)

A 500-mL jacketed three-necked round-bottom flask equipped with a magnetic stir bar was charged with two equivalents of **3** (19.8 g, 0.0933 mol) and 370 mL of glacial acetic acid. Next, two equivalents of $KBrO_3$ (15.7 g, 0.0940 mol) were dissolved in deionized water with heating and added to the acetic acid slurry. The reaction mixture was stirred for 16 h at 50°C and resulted in formation of a yellow precipitate and dark orange solution. The precipitate was collected by filtration on a Büchner funnel and washed with a small amount of cold glacial acetic acid (∼50 mL). The yellow precipitate was resuspended in deionized water (∼200 mL) to dissolve any unreacted $KBrO_3$ and filtered again on a Büchner funnel, washed with deionized water (3×50 mL), and dried under vacuum to give ADAAF (**4**, 11.5 g, 0.027 mol) in 60% isolated yield. X-ray quality crystals of **4** can be obtained from hot CH_3CN. ^{1}H NMR (300 MHz, RT, $(CD_3)_2SO$) 7.03 (s, br, NH_2). $^{13}C\{^1H\}$ NMR (75.57 MHz, RT, $(CD_3)_2SO$) 159.2, 151.9, 151.3, 147.1. Anal. Calcd. for $C_8H_4N_{16}O_6$: C, 22.87; H, 0.96; N, 53.33. Found: C, 23.10; H, 1.012; N, 53.10. $\Delta H_f = 300$ kcal/mol.

3,4:7,8:11,12:15,16-Tetrafurazano-1,2,5,6,9,10,13,14-Octaazacyclohexadeca-1,3,5,7,9,11,13,15-Octaene-1,10-Dioxide (DOATF, 5)

A 3-L round-bottom flask equipped with a magnetic stir bar was charged with one equivalent of **4** (5.3 g, 0.013 mol) and

1.9 L of CH_3CN. To this slurry was added 1.9 equivalents of TCI (trichloroisocyanuric acid, 5.6 g, 0.024 mol). Within one hour, the orange slurry became an orange solution that was stirred overnight at room temperature (∼22°C). Next, the CH_3CN was removed under vacuum to give an orange powder that was redissolved in toluene (75 mL) and filtered through Celite on a Büchner funnel (washed with toluene, 2×10 mL). The toluene solution was then concentrated and chromatographed on silica gel with CH_2Cl_2:hexanes (2:1) and recrystallized from warm toluene to give orange X-ray quality crystals of DOATF (**5**, 1.4 g, 0.0034 mol) in 26% isolated yield. M.P. 127°C. $^{13}C\{^1H\}$ NMR (75.57 MHz, RT, CD_3CN): δ 159.6, 157.7, 154.5, 150.0. Anal. Calcd. for $C_8N_{16}O_6$: C, 23.09; H, 0.00; N, 53.85. Found: C, 23.20; H, 0.030; N, 53.30.

Acknowledgments

The authors thank Dan Hooks for helpful discussion related to crystal packing; Stephanie Hagelberg for elemental analyses; Mary Sandstrom and Geoff Brown for thermal analyses; Daniel Preston, Gabe Avilucea, and Ernie Hartline for sensitivity tests; Joe Lloyd, Eric Sanders, and Dennis Montoya for performance testing; and Dave Oschwald for assistance with burning rate studies. This work was supported by the DoD/DOE Joint Munitions Technology Development Program.

References

[1] Coburn, M. D. 1968. Picrylamino-substituted heterocycles. II. Furazans. *Journal of Heterocyclic Chemistry*, 5: 83.

[2] Solodyuk, G. D., M. D. Boldyrev, B. V. Gidaspov, and V. D. Nikolaev. 1981. Oxidation of 3,4-diaminofurazan by some peroxide reagents. *Zh. Org. Khim.*, 17: 756.

[3] Novikova, T. S., T. M. Mel'nikova, O. V. Kharitonova, V. O. Kulagina, N. S. Aleksandrova, A. B. Sheremetev, T. S. Pivina, L. I. Khmel'nitskii, and S. S. Novikov. 1994. An effective method for the oxidation of aminofurazans to nitrofurazans. *Mendeleev Communications*, 4: 138.

[4] Gunasekaran, A., T. Jayachandran, J. H. Boyer, and M. L. Trudell. 1995. A convenient synthesis of diaminoglyoxime and diaminofurazan: Useful precursors for the synthesis of high density energetic materials. *Journal of Heterocyclic Chemistry*, 32: 1405.

[5] Batog, L. V., L. S. Konstantinova, O. V. Lebedev, and L. I. Khmel'nitskii. 1996. Hypohalites as reagents for the macrocyclization of diamines of the furazan series. *Mendeleev Communications*, 5: 193.

[6] Batog, L. V., V. Y. Rozhkov, L. S. Konstantinova, V. E. Eman, M. O. Dekaprilevich, Y. T. Struchkov, S. E. Semenov, O. V. Lebedev, and L. I. Khel'nitskii. 1996. Oxidative macrocyclocondensation of 3,4-diaminofurazan and 4,4′-diamino-3,3′-azofurazan with dibromoisocyanurate. Crystal structures of hexa- and octadiazenofurazan macrocycles. *Russian Chemical Bulletin*, 45: 1189.

[7] Eman, V. E., M. S. Sukhanov, O. V. Lebedev, L. V. Batog, L. S. Konstantinova, V. Y. Rozhkov, and L. I. Khmel'nitskii. 1996. Polydiazenofurazans: Novel macrocyclic systems. *Mendeleev Communications*, 2: 66.

[8] Batog, L. V., L. S. Konstantinova, V. E. Eman, M. S. Sukhanov, A. S. Batsanov, Y. T. Struchkov, O. V. Lebedev, and L. I. Khmel'nitskii. 1996. Novel method for synthesis of 3,4:7,8:11,12:15,16-tetrafurazano-1,2,5,6,9,10,13,14-octaazacyclohexadeca-1,3,5,7,9,11,13,15-octaene and its crystal structure. *Chemistry of Heterocyclic Compounds*, 32: 352.

[9] Eman, V. A., M. S. Sukhanov, O. V. Lebedev, L. V. Batog, L. S. Konstantinova, V. Y. Rozhkov, M. O. Dekaprilevich, Y. T. Struchkov, and L. I. Khmel'nitskii. 1997. First representatives of macrocyclic poly(diazene oxide furazans): 3,4:7,8:11,12:15,16-Tetrafurazano-1,2,5,6,9,10,13,14-octaazacyclohexadeca-1,3,5,7,9,11,13,15-octaene 1,9-and 1,10-dioxides; 1,5,9,13-tetraoxide and its crystal structure. *Mendeleev Communications*, 7: 5.

[10] (a) Chavez, D. E., L. Hill, M. Hiskey, and S. Kinkead. 2000. Preparation and explosive properties of azo- and azoxy-furazans. *Journal of Energetic Materials*, 18: 219. (b) Francois, E. G., D. E. Chavez, and M. M. Sandstrom. In press. The development of a new synthesis process for 3,3′diamino-4,4′azoxyfurazan (DAAF). *Propellants, Explosives, Pyrotechnics*. (c) Francois, E. G., D. E. Chavez, J. T. Mang, V. E. Sanders, and J. M. Lloyd, Processing and Sensitivity characteristics of diaminoazoxyfurazan

(DAAF). In *Proceedings of the 35th JANNAF Propellant and Explosives Development and Characterization Subcommittee Meeting*, Las Vegas, NV, April 14–17, 2009.

[11] Sheremetev, A. B., N. S. Aleksandrova, and V. O. Kulagina. 2005. Method for preparing 4,4′-bis-[4-aminofurazan-3-yl-N(O)N-azoxy]-3,3′-azofurazine and its applying as thermostable explosive substance. Russian Patent Application RU2248354.

[12] Sheremetev, A. B., V. O. Kulagina, I. A. Kryazhevskikh, T. M. Melnikova, and N. S. Aleksandrova. 2002. Nucleophilic substitution in the furazan series. Reactions of nitrofurazans with ammonia. *Russian Chemical Bulletin, International Edition*, 51: 1533.

[13] Li, Z., S. Tang, and W. Wang. 2007. Synthesis and property of furazan macrocyclic compounds TATF and DOATF. *Hanneng Cailiao*, 15: 6.

[14] Chen, F.-E., Y.-Y. Kuang, H.-F. Dai, L. Lu, and M. Huo. 2003. A selective and mild oxidation of primary amines to nitriles with trichloroisocyanuric acid. *Synthesis*, 17: 2629.

[15] (a) Gilardi, R. 1999. Private communication. The Cambridge Structural Database. (b) Allen, F.H. *Acta Crystallographica*, B58: 380–388, 2002.

[16] Beal, R. W., C. D. Incarvito, B. J. Rhatigan, A. L. Rheingold, and T. B. Brill. 2000. X-ray crystal structures of five nitrogen-bridged bifurazan compounds. *Propellants, Explosives, Pyrotechnics*, 25: 277.

[17] Cady, H. H. and A. C. Larson. 1965. The crystal structure of 1,3,5-triamino-2,4,6-tribitrobenzene. *Acta Crystallographica*, 18: 485.

[18] (a) Fried, E., K. R. Glaesemann, W. M. Howard, and P. C. Souers. 2004. *CHEETAH 4.0 User's Manual*. Livermore, CA: Lawrence Livermore National Laboratory. (b) Lu, J. P. 2001. *Evaluation of the Thermochemical Code—CHEETAH 2.0 for Modelling Explosives Performance*. Edinburgh: DSTO. DSTO-TR-1199.

[19] (a) Tappan, B. C., A. N. Ali, and S. F. Son. 2006. Decomposition and ignition of the high-nitrogen compound triaminoguanidinium azotetrazolate (TAGzT). *Propellants, Explosives, Pyrotechnics*, 31: 163. (b) Son, S. F., H. L. Berghout, C. A. Bolme, D. E. Chavez, D. Naud, and M. A. Hiskey. 2000. Burn rate measurements of HMX, TATB, DHT, DAAF, and BTATz.

Proceedings of the Combustion Institute, 28: 919. (c) Ward, M. J., S. F. Son, and M. Q. Brewster. 1998. Steady deflagration of HMX with simple kinetics: A gas phase chain reaction model. *Combustion and Flame*, 114: 556.
[20] Bruker. 2001a. *SMART*, v5.625. Madison, WI: Bruker AXS Inc.
[21] Bruker. 2002. *SAINT*, v6.45A. Madison, WI: Bruker AXS Inc.
[22] Bruker. 2001b. *XPREP*, v6.14. Madison, WI: Bruker AXS Inc.
[23] Bruker. 2000. *SADABS*, v2.10. Madison, WI: Bruker AXS Inc.
[24] Bruker. 2000. *SHELXTL*, v6.12. Madison, WI: Bruker AXS Inc.